Energy 257 (2022) 124776

Contents lists available at ScienceDirect

Energy

journal homepage: www.elsevier.com/locate/energy

Analysis of a direct vapor generation system using cascade steam-organic Rankine cycle and two-tank oil storage

Pengcheng Li [a, c], Haiwei Lin [a], Jing Li [b, *], Qing Cao [d], Yandong Wang [e], Gang Pei [f], Desuan Jie [a], Zilong Zhao [a]

[a] School of Automotive and Transportation Engineering, Hefei University of Technology, 193 Tunxi Road, Hefei, China
[b] Research Center for Sustainable Energy Technologies, Energy and Environment Institute, University of Hull, Hull, HU6 7RX, UK
[c] DONGFANG ELECTRIC Dongfang Boiler Group CO., LTD., 150 Huangjue Ping, Wuxing Street, Zigong, China
[d] School of Mechanical Engineering, Hefei University of Technology, 193 Tunxi Road, Hefei, China
[e] Hefei General Machinery Research Institute, 888 Changjiang Road, Hefei, China
[f] Department of Thermal Science and Energy Engineering, University of Science and Technology of China, 96 Jinzhai Road, Hefei, China

ARTICLE INFO

Article history:
Received 22 January 2022
Received in revised form
19 June 2022
Accepted 6 July 2022
Available online 15 July 2022

Keywords:
Direct vapor generation
Cascade steam-organic Rankine cycle
Thermal oil storage
Heat discharge
Equivalent payback period

ABSTRACT

A direct vapor generation solar power system using cascade steam-organic Rankine cycle and two-stage oil tanks is proposed. It offers a significantly enlarged storage capacity due to the unique discharge operation mode. Synthetic oil Therminol® VP-1 is used as the heat carrier and storage medium. Compared with the direct steam generation system, the steam turbine inlet temperature is elevated from 270 °C to 311 °C. Thermodynamic analysis indicates that the optimal equivalent heat-to-power conversion efficiency ($\eta_{eq,opt}$) is 27.91% when benzene is used as the bottom fluid and the mass of oil is 1000 tonnes. $\eta_{eq,opt}$ is raised by 7.72−11.60% for the selected four organic fluids as compared with the direct steam generation type. The temperature drop of oil during discharge can reach about 280 °C. Economic studies demonstrate that the proposed system is more cost-effective. Its equivalent payback period is less than 5 years for a 10 MW system with 2000 tonnes of oil. Further investigation shows that it is also more advantageous than a conventional thermal oil-based indirect solar power system due to the cost reduction in heat storage.

1. Introduction

Direct steam generation (DSG) is an effective method to reduce the levelized electricity cost and irreversible losses of concentrated solar power (CSP) plants. However, some inherent barriers must be tackled before this technology is popularized and applied on a large scale. These include expensive long-term storage [1] and complicated control strategies due to flashing during the discharge process [2]. The DSG systems using cascade steam-organic Rankine cycle (SORC)/cascade organic Rankine cycle (CORC) and dual-tank steam storage have considerable potential to solve or alleviate the above challenges [3–5]. The schematic diagram of the SORC is illustrated in Fig. 1. In normal working conditions, water in the low-temperature accumulator (LTA) is heated and partially vaporized by solar collectors. The saturated steam in the high-temperature accumulator (HTA) is used to drive the SORC, and the hot water is stored in the HTA. Stable power conversion can be facilitated by adjusting the mass flow of water from the LTA to HTA according to solar radiation. During discharge, the stored hot water moves from the HTA into LTA and the released heat is used only to drive the bottom organic Rankine cycle (ORC). The storage capacity can be remarkably elevated due to the unique two-tank structure. The optimization of steam condensation temperature has been conducted [6], followed by the impact study of a regenerator on the system performance [7]. In the above systems, water acts as both the heat transfer and storage medium, as well as the working fluid of the top steam Rankine cycle (SRC) in Fig. 1. A high inlet temperature of the steam turbine is more beneficial from the viewpoint of power conversion. Nevertheless, the steam generation temperature in the parabolic trough collectors (PTCs) of the DSG systems is generally limited to 250 °C [4,5,7] or 270 °C [3,6] on account of the following two reasons.

First, in terms of heat storage, storing steam at high temperature and pressure leads to a surge in steel thickness and processing cost

* Corresponding author.
E-mail address: Jing.Li@Hull.ac.uk (J. Li).

https://doi.org/10.1016/j.energy.2022.124776

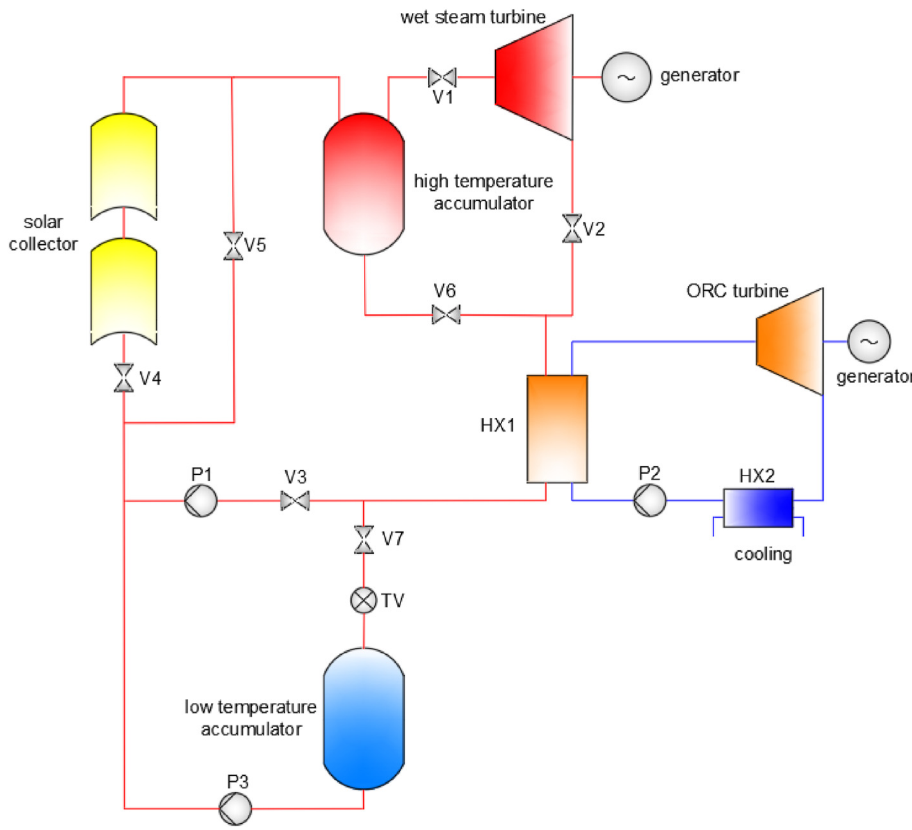

Fig. 1. DSG system using two-stage steam accumulators and SORC.

for the tanks. The steam pressure in the vessels is merely 4.5 MPa for Planta Solar 10 and Planta Solar 20, and it is 5.5 MPa for Puerto Errado 1 and Puerto Errado 2 [3,8]. The corresponding saturation temperature is 257 °C and 270 °C, respectively. The saturation pressure will rise significantly at higher temperatures. For example, it is 6.9 MPa at 285 °C and 8.6 MPa at 300 °C.

Second, in terms of heat collection, the sealability between the glass sleeve and the metallic absorber tubes, and the interconnection reliability between the collectors and tubes cannot be guaranteed at high temperature and pressure [9]. The thickness of the metallic absorber tubes produced by the major manufacturers worldwide is generally 2 mm and the bearing capacity is limited to 4 MPa [10,11]. For instance, the PTCs of the 5 MW Thai Solar Energy 1 produce 3 MPa live steam [12]. The 2 MW Stillwater GeoSolar Hybrid Plant uses demineralized water as heat transfer fluid [13], and the pressure is 310 psi (about 2.1 MPa) [14]. Although there are exceptions: the produced steam was at 7 MPa/410 °C and 10 MPa/400 °C respectively in the demonstration DSG projects of INDITEP [15] and DISS [16]. The absorber tubes were specially designed with an inner/outer diameter of 0.055/0.07 m and a thickness of 7.5 mm [15] and 10 mm [16] respectively, which inevitably resulted in huge steel costs and fabrication expenses. These specially designed tubes were no longer used in the subsequent DSG projects.

The selection of appropriate heat transfer and storage medium emerges as a key issue in CSP plants. A typical synthetic oil Therminol® VP-1 (composed of 26.5% biphenyl and 73.5% diphenyl oxide) has been adopted in SEGS II ~ IX for decades [8]. Its saturation pressure is merely 1.09 MPa at 400 °C [17]. The design pressure at the solar field inlet has been set at 2.5 MPa to avoid evaporation at the outlet [18]. It combines exceptional thermal stability and low viscosity for efficient, dependable, uniform performance in a wide use range of 12 °C–400 °C, and can be utilized as a liquid or boiling-condensing heat transfer medium up to 400 °C [19].

If the synthetic oil is in place of water in the DSG systems for heat transfer and storage, the technical defects associated with high-pressure steam can be resolved owing to the extremely low pressure of oils. On this basis, a direct vapor generation (DVG) system using two-stage oil tanks and SORC is proposed as exhibited in Fig. 2. To the best knowledge of the authors, it is the first time that the oil-based dual tanks have been combined with the SORC for CSP application. Unlike the thermal oil of a conventional CSP system in liquid state, the oil in the proposed system is vaporized in the solar field. The oil acts as both heat carrier and storage fluid, while water is still utilized for power generation in the top SRC.

The proposed DVG-SORC system has a few clear advantages. First, compared with the DSG-SORC [3] or DSG-CORC system [5], it has a higher thermal efficiency due to a higher evaporation temperature of the top SRC. The pressure-bearing problems in both the accumulators and the absorber tubes are greatly alleviated. The life expectancy of the tubes will be longer and the initial investment in the tanks will be smaller. Second, it can offer more efficient heat collection than a conventional PTC system using synthetic oil. The collectors benefit from constant temperature and a high heat transfer coefficient in the binary-phase region as the oil evaporates directly in PTCs. Third, in the discharge process the oil is employed to drive the bottom ORC and the temperature difference between the HTA and LTA can be significantly increased, leading to a larger storage capacity at a given mass of oil. Fourth, the problems of high condensation temperature, limited storage capacity and fluctuant vapor generation rate inhered in DVG-ORC systems with single-tank configuration [2,20–23] are also eliminated.

The operating principles and characteristics of the proposed DVG-SORC system are elaborated. Mathematical models are built.

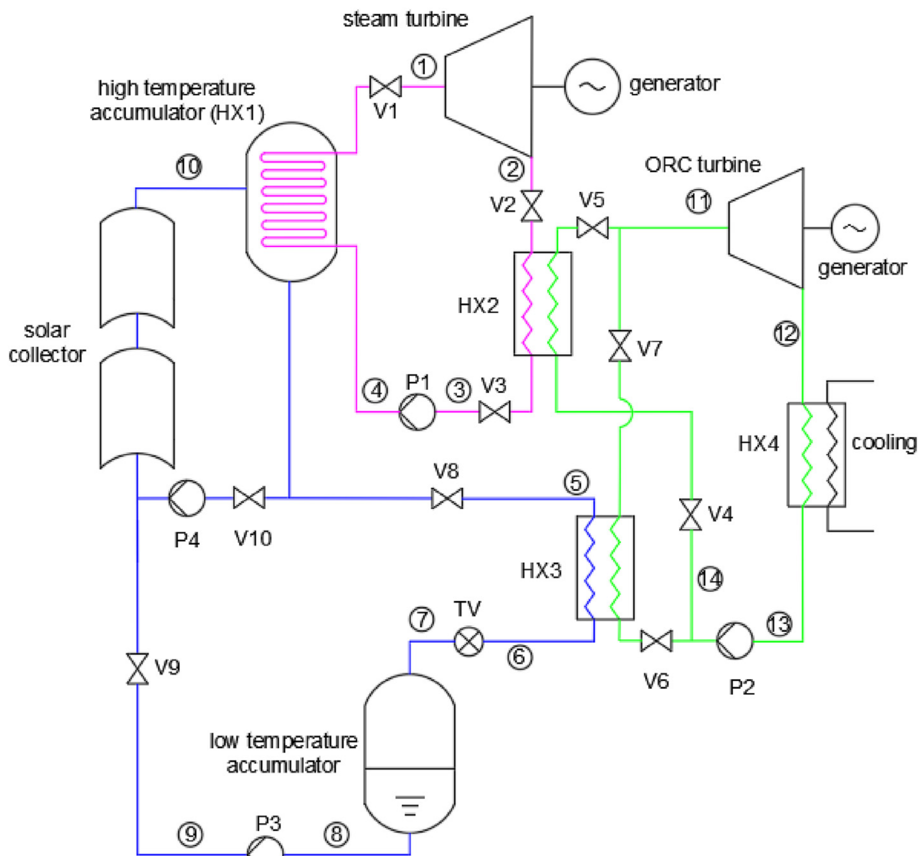

Fig. 2. DVG system using two-tank oil storage and SORC.

Thermodynamic analysis on two typical modes is conducted, followed by an economic performance assessment. A comparison with the DSG-SORC and conventional thermal oil solar systems is made.

2. System description

Fig. 2 shows the schematic diagram of the DVG-SORC system. It consists of three loops: the left oil cycle in blue, the top SRC in magenta and the bottom ORC in green. The oil cycle is composed of PTCs, HTA, LTA, heat exchanger 3 (HX3), pumps (P3 and P4). The top SRC mainly comprises a steam turbine, condenser (HX2), and a water pump (P1). The evaporator for the top SRC is a coiled pipe heat exchanger (i.e., HX1) placed inside the HTA. The bottom ORC includes an ORC dry turbine, condenser (HX4), and an organic fluid pump (P2).

Depending on the direct normal solar irradiance (I_{DN}), the system can operate in several modes. Two main modes are marked in red lines in Fig. 3 and the operating fundamentals are described as follows.

Fig. 4 shows the power output of the proposed system throughout a typical day. Stable power conversion over a wide range of solar radiation is guaranteed. When the solar radiation is higher than 400 W/m^2, the vapor generation rate is constant while the residual solar heat is stored in the HTA. At weaker solar radiation, the system uses the bottom ORC for power conversion with a constant output. Thanks to the decoupled power cycles in the charge and discharge modes, it overcomes the challenges of conventional DSG systems under fluctuating radiation.

3. Mathematical models

3.1. Thermodynamics

3.1.1. Solar field

The solar heat collection is simulated by the System Advisor Model (SAM) software, which is developed by National Renewable Energy Laboratory [24].

PTC efficiency (η_{PTC}) is defined as the optical efficiency (η_{opt}) minus an efficiency penalty term (η_{loss}) representing heat loss [24]:

$$\eta_{PTC} = \eta_{opt} - \eta_{loss} = K\eta_{opt,0} - \frac{Lcq_{loss,av}}{A_{PTC} \cdot I_{DN}} \tag{1}$$

where K denotes the dependency of η_{opt} on the incidence angle; $\eta_{opt,0}$ is the peak optical efficiency when the incidence angle is zero; L is the length of receivers (m); $q_{loss,av}$ is the average heat loss from evacuated tube receivers (W/m); A_{PTC} is the aperture area (m^2).

$q_{loss,av}$ is evaluated by Ref. [24]:

$$q_{loss,av} = a_0 + a_5\sqrt{v_W} + (a_1 + a_6\sqrt{v_W}) \cdot \frac{T_{in} + T_{out} - T_a}{2} + (a_2 + a_4 I_{DN} K) \cdot \frac{T_{in}^2 + T_{in} \cdot T_{out} + T_{out}^2}{3} + a_3 \frac{\left(T_{in}^2 + T_{out}^2\right)(T_{in} + T_{out})}{4} \tag{2}$$

where $a_0 \ldots a_6$ are the heat loss coefficients; v_w is the wind speed (m/s); T_{in} and T_{out} are the inlet and outlet temperatures of PTCs (°C); T_a is the ambient temperature (°C).

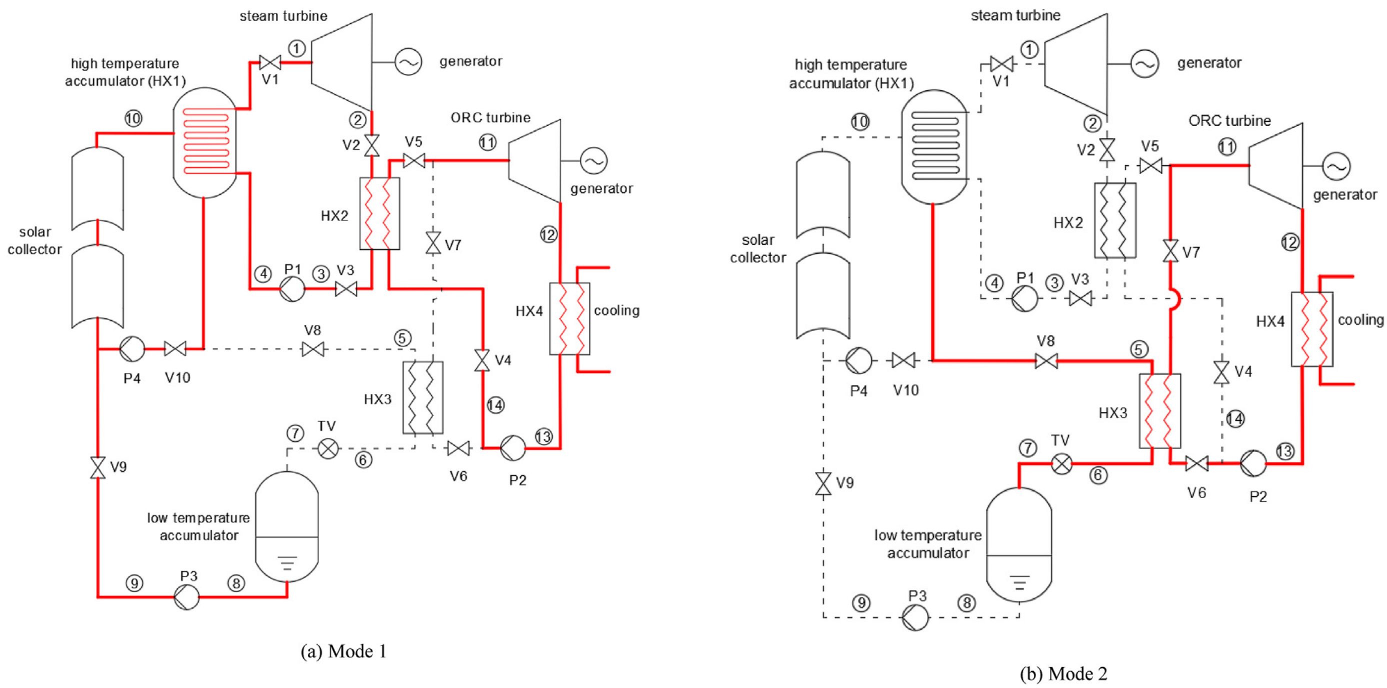

Fig. 3. Flow diagrams for two typical modes: (a) Mode 1; (b) Mode 2. (a) Mode 1 Mode 1: Simultaneous heat collection and SORC power conversion. It is assumed that when I_{DN} in the design condition is 400 W/m^2, the solar heat gain equals the rated heat input of the SORC. The system operates in Mode 1 when I_{DN} >400 W/m^2. Power is produced through SORC. All the pumps are operational. V1–V5, V9 and V10 are open. Liquid oil leaving LTA is heated and partially vaporized in PTCs. It is in a binary phase state at the HTA inlet (point 10) and the function of P4 is to control its dryness depending on I_{DN}. The binary phase oil is the mixture of saturated vapor with a constant flow rate and saturated liquid with a variable flow rate. The former evaporates the water in the coiled pipe of HX1 and the produced saturated steam is used to drive the SORC, while the latter is stored in HTA with the condensed liquid. (b) Mode 2. Mode 2: Heat discharge. V6–V8 and TV are open. P2 is operational. The dissipated hot oil in HTA flows into LTA via HX3, and the released heat is used only to drive the bottom ORC.

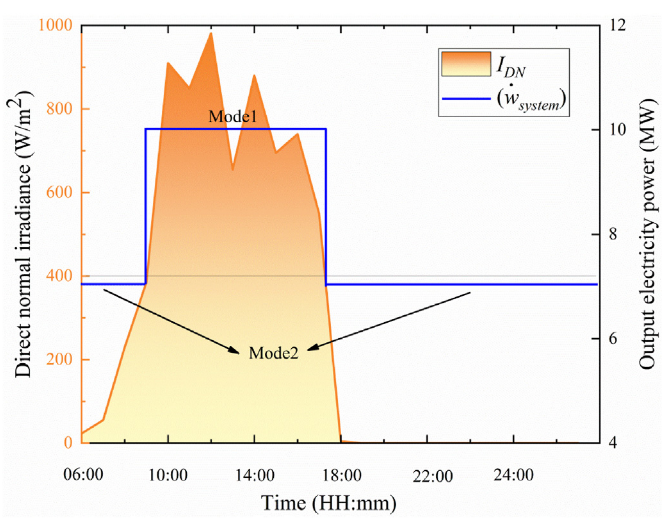

Fig. 4. Variations of direct normal irradiance and operation modes throughout the day.

The collectors consist of liquid and binary phase regions. The collector outlet can be a steam-liquid mixture of different dryness with the variation of I_{DN}, and η_{PTC} will change accordingly. The collector efficiency in liquid phase region ($\eta_{PTC,\ l}$) is appraised by

$$\eta_{PTC,\ l} = \frac{\dot{m}_{oil} \cdot \Delta h_l}{I_{DN} \cdot A_l} \tag{3}$$

where $\dot{m}_{oil}$ is the mass flow rate of the oil.

The actual overall collector efficiency is

$$\eta_{PTC} = \frac{Q}{I_{DN} \cdot A} = \frac{Q_l + Q_b}{I_{DN} \cdot (A_l + A_b)} = \frac{\dot{m}_{oil} \cdot \Delta h_l + \dot{m}_{oil} \cdot \Delta h_b}{\frac{\dot{m}_{oil} \cdot \Delta h_l}{\eta_{PTC,\ l}} + \frac{\dot{m}_{oil} \cdot \Delta h_b}{\eta_{PTC,\ b}}} = \frac{\Delta h_l + \Delta h_b}{\frac{\Delta h_l}{\eta_{PTC,\ l}} + \frac{\Delta h_b}{\eta_{PTC,\ b}}} \tag{4}$$

where Δh_l and Δh_b are the enthalpy increments of the oil in liquid phase and binary phase regions. The specific parameters and the corresponding default values are indexed in Table 1.

K is calculated by Ref. [24]:

$$K_{PTC} = IAM_{PTC} \cos\theta = min\left(1,\ \frac{c_0 \cos\theta + c_1\theta + c_2\theta^2}{\cos\theta}\right)\cos\theta \tag{5}$$

where IAM_{PTC} represents the incidence angle modifier; θ is the incidence angle (°) and its calculation procedure can be referred to

Table 1
Specific parameters of PTCs in SAM [24].

Term	PTCs
Receiver length, L	150 m
Aperture area, A_{col}	817.5 m^2
Optical efficiency, η_{opt}	76.77%
Heat loss coefficient, C_0	4.05
Heat loss coefficient, C_1	0.247
Heat loss coefficient, C_2	−0.00146
Heat loss coefficient, C_3	5.65e-06
Heat loss coefficient, C_4	7.62e-08
Heat loss coefficient, C_5	−1.7
Heat loss coefficient, C_6	0.0125

the author's previous work [3,7]; c_0, c_1 and c_2 are the incidence angle coefficients.

3.1.2. Turbines

The work generated by the wet steam and ORC dry turbines is determined by

$$\dot{w}_{ST} = \dot{m}_{SRC}(h_1 - h_2) = \dot{m}_{SRC}(h_1 - h_{2s})\varepsilon_{ST} \tag{6}$$

$$\dot{w}_{OT} = \dot{m}_{ORC}(h_5 - h_6) = \dot{m}_{ORC}(h_5 - h_{6s})\varepsilon_{OT} \tag{7}$$

where ε_{ST} and ε_{OT} are respectively the isentropic efficiencies of the wet steam and ORC dry turbines. ε_{OT} is a constant because the ORC turbine is operated without liquid droplets. ε_{ST} is associated with steam wetness, as described by the Baumann rule [25].

$$\varepsilon_{ST} = \varepsilon_{ST,sh}(1 - a y_{av}) \tag{8}$$

$$y_{av} = (y_1 + y_2)/2 \tag{9}$$

where $\varepsilon_{ST,sh}$ is the reference isentropic efficiency assuming that the turbine works with superheated steam; a is the Baumann factor, which usually ranges from 0.4 to 2.0 [26]; y_1 and y_2 are the main steam and exhaust steam wetness, respectively.

Given the main steam and steam condensation temperature, h_1, h_{2s} and y_1 are determined. y_2 can be derived by combining Eqs. (8)-9)

$$\varepsilon_{ST} = \frac{h_1 - h_2}{h_1 - h_{2s}} = \frac{h_1 - [y_2 h_{2,l} + (1 - y_2)h_{2,v}]}{h_1 - h_{2s}} \tag{10}$$

The result is

$$y_2 = \frac{\varepsilon_{ST,sh}(2 - a y_1)(h_1 - h_{2s}) - 2(h_1 - h_{2,v})}{\varepsilon_{ST,sh} a(h_1 - h_{2s}) - 2(h_{2,l} - h_{2,v})} \tag{11}$$

where $h_{2,l}$ and $h_{2,v}$ are the saturated liquid and vapor enthalpy at T_2 separately.

3.1.3. Heat exchangers

The heat balance in HX2 and HX3 is determined by

$$\dot{m}_{SRC}(h_2 - h_3) = \dot{m}_{ORC}(h_{11} - h_{14}) \tag{12}$$

$$\dot{m}_{oil}(h_5 - h_6) = \dot{m}_{ORC}(h_{11} - h_{14}) \tag{13}$$

The minimum temperature difference (ΔT_{min}) of HX3 may occur at two places:

1) If ΔT_{min} takes place at the pinch point, then the heat balance in the binary phase region is determined by

$$\dot{m}_{oil}\left(h_5 - h_{oil,pinch}\right) = \dot{m}_{ORC}(h_{11} - h_{11,l}) \tag{14}$$

where $h_{oil,pinch}$ is the pinch point enthalpy of oil at the temperature of ($T_{11} + \Delta T_{min}$); $h_{11,l}$ is the saturated liquid enthalpy of organic fluid at T_{11}.

2) If ΔT_{min} occurs at the oil outlet, then T_6 is obtained by

$$T_6 = T_{14} + \Delta T_{min} \tag{15}$$

3.1.4. Pumps

The work consumed by P1 and P2 is calculated by

$$\dot{w}_{P1} = \dot{m}_{SRC}(h_4 - h_3) = \dot{m}_{SRC}(h_{4s} - h_3)\,/\,\varepsilon_P \tag{16}$$

$$\dot{w}_{P2} = \dot{m}_{ORC}(h_{14} - h_{13}) = \dot{m}_{ORC}(h_{14s} - h_{13})\,/\,\varepsilon_P \tag{17}$$

where ε_P is the pump isentropic efficiency.

The oil flows from HTA to LTA continuously in the discharge process to drive the ORC. For further circulation, it is necessary to pump back the oil into HTA to supplement the diminishing mass. The required power is defined as

$$\dot{w}_{P3} = \dot{m}_{oil}(h_9 - h_8) = \dot{m}_{oil}(h_{9s} - h_8)\,/\,\varepsilon_P \tag{18}$$

3.1.5. Thermodynamic states of the oil

The thermophysical properties of synthetic oil Therminol® VP-1 cannot be acquired from REFPROP, but its saturated state parameters at intervals of 10 °C can be obtained from a supplier Eastman Corp [17]. The parameters in saturated state at any temperature (like T, p, h, v) can be calculated by linear interpolation. The enthalpy values of unsaturated states can be derived from the thermodynamic differential equation

$$dh = c_p dT + \left[v - T\left(\frac{\partial v}{\partial T}\right)_p\right]dp \tag{19}$$

The saturated enthalpy h_5 can be calculated by linear interpolation ($h_5 = 603.78$ kJ/kg). The pressure drop in all HXs is negligible. $h_{oil,pinch}$ can be deduced by integrating Eq. (19).

$$h_5 - h_{oil,pinch} = \int_{T_{oil,pinch}}^{T_5} c_p dT \tag{20}$$

where c_p is the subcooled specific heat capacity. c_p in each degree Celsius integral interval can be approximately replaced by the average of the initial and final saturated liquid specific heat capacities.

h_6 can be obtained according to Eq. (14) if ΔT_{min} takes place at the pinch point of HX3. Analogously, given the enthalpy variation, unsaturated temperatures can also be acquired from Eq. (19). T_6 can be deduced by

$$h_5 - h_6 = \int_{T_6}^{T_5} c_p dT \tag{21}$$

Most ORC fluids at a liquid state are not compressible, and most of the heat is taken out by the condensation process [27]. Therefore,

$$h_{9s} \approx h_8 + v_8(p_{9s} - p_8) \tag{22}$$

where $p_{9s} = p_9 = p_{10} = 0.3461$ MPa (p_{10} can be derived from T_{10} by linear interpolation and $T_{10} = T_1 + \Delta T_{min}$). The parameters of saturation state h_8, v_8 and p_8 can be obtained by linear interpolation as well.

3.1.6. Normal operation performance

Thermal efficiencies of the SRC, ORC and SORC are expressed by

$$\eta_{SRC} = \frac{\dot{w}_{SRC}}{\dot{m}_{SRC}(h_1 - h_4)} = \frac{\dot{w}_{ST}\varepsilon_g - \dot{w}_{P1}}{\dot{m}_{SRC}(h_1 - h_4)} \tag{23}$$

$$\eta_{ORC}=\frac{\dot{w}_{ORC}}{\dot{m}_{ORC}(h_{11}-h_{14})}=\frac{\dot{w}_{OT}\varepsilon_g-\dot{w}_{P2}}{\dot{m}_{ORC}(h_{11}-h_{14})} \tag{24}$$

$$\eta_{SORC}=\frac{\dot{w}_{SORC}}{\dot{m}_{SRC}(h_1-h_4)}=\frac{\dot{w}_{SRC}+\dot{w}_{ORC}}{\dot{m}_{SRC}(h_1-h_4)} \tag{25}$$

where ε_g is the generator efficiency.

3.1.7. Heat discharge performance

3.1.7.1. Operating time of the bottom ORC. For a certain amount of storage oil, the operating time of Mode 2 (t_{ORC}, i.e., the storage capacity) is defined as

$$t_{ORC}=\frac{M_{oil}}{\dot{m}_{oil}} \tag{26}$$

where M_{oil} is the mass of stored oil; $\dot{m}_{oil}$ is derived from Eqs. (13) and (14).

3.1.7.2. Annual power output during discharge. Annual power output during discharge ($W_{DVG,d}$) is calculated as

$$W_{DVG,d}=365\cdot t_{ORC}\cdot \dot{w}_{ORC,d} \tag{27}$$

$$\dot{w}_{ORC,d}=\dot{w}_{OT}\varepsilon_g-(\dot{w}_{P2}+\dot{w}_{P3}) \tag{28}$$

3.1.7.3. Bottom ORC efficiency. The bottom ORC efficiency during the discharge process ($\eta_{ORC,d}$) is determined as

$$\eta_{ORC,\,d}=\frac{\dot{w}_{ORC,d}}{\dot{m}_{ORC}(h_{11}-h_{14})}=\frac{\dot{w}_{OT}\varepsilon_g-(\dot{w}_{P2}+\dot{w}_{P3})}{\dot{m}_{ORC}(h_{11}-h_{14})} \tag{29}$$

$\eta_{ORC,\,d}$ is slightly lower than η_{ORC} as expressed by Eq. (24) owing to the consumption of $\dot{w}_{P3}$. The reason that $\dot{w}_{P3}$ shall be taken into account in $\eta_{ORC,d}$ but not in η_{ORC} has been clarified [5].

3.1.8. Equivalent heat-to-power conversion efficiency

The equivalent heat-to-power conversion efficiency (η_{eq}) combines the efficiencies in the two modes [6]. It is appraised by

$$\eta_{eq}=\frac{\dot{w}_{total}}{\dot{q}_{total}}=\frac{t_{SORC}\dot{w}_{SORC}+t_{ORC}\dot{w}_{ORC,d}}{t_{SORC}\cdot\dot{m}_{RC}(h_1-h_4)+t_{ORC}\cdot\dot{m}_{ORC}(h_5-h_8)} \tag{30}$$

where t_{SORC} is the operating time of SORC and it is determined by the duration of irradiation. η_{eq} comprehensively reflects the SORC system performance. From the viewpoint of thermodynamics, η_{eq} indicates how effectively the absorbed solar energy, including that stored in HTA, is converted into electricity.

3.2. Thermo-economics

An evaluation of the cost and payback time of the entire system is not conducted due to its complexity. Instead, the economic advantages of the proposed system will be revealed as compared with the system in Fig. 1. The DVG-SORC system can facilitate excess power generation per year at the expense of additional investment. An equivalent payback period (*EPP*) is defined as

$$EPP=\frac{C_{add}}{Y} \tag{31}$$

where C_{add} is the extra cost, which includes supplementary investments in PTCs, accumulators, HX3 and the oil. *Y* is the excess annual yield.

For the convenience of comparison, the runtime of the rated mode (t_{SORC}) for both systems is 8 h *Y* consists of the output difference under both modes. Determining the *EPP* is reasonable by

$$EPP=\frac{\Delta C_{PTC}+\Delta C_{accumulator}+C_{HX3}+C_{oil}}{(Y_{DVG,\,rated}-Y_{DSG,\,rated})+(Y_{DVG,\,d}-Y_{DSG,\,d})} \tag{32}$$

Each term in Eq. (32) is explained as follows.

3.2.1. Supplementary investments in PTCs (ΔC_{PTC})

The aggregate aperture area includes the area required by the two modes. Accordingly, ΔC_{PTC} is divided into two parts.

$$\Delta C_{PTC}=P_{PTC}\cdot\Delta A=P_{PTC}\cdot[\times(A_{DVG,\,rated}-A_{DSG,\,rated})+(A_{DVG,\,d}-A_{DSG,\,d})] \tag{33}$$

where P_{PTC} is the PTC price. *A* is the required PTC area.

A_{DVG} is individually expressed by

$$A_{DVG,\,rated}=\frac{t_{SORC}\cdot\dot{m}_{RC}(h_1-h_4)}{t_{s,\,st}\cdot I_{DN,\,st}\cdot\eta_{PTC,\,DVG}} \tag{34}$$

$$A_{DVG,\,d}=\frac{M_{VP-1}\cdot(h_5-h_6)}{t_{s,\,st}\cdot I_{DN,\,st}\cdot\eta_{PTC,\,l,\,DVG}} \tag{35}$$

where $t_{s,\,st}$ is the standard sunshine duration (h); $I_{DN,\,st}$ is the standard direct normal solar irradiance (kW/m^2) and $\eta_{PTC,\,DVG}$ is the PTC efficiency corresponding to the optimal η_{eq}.

3.2.2. Supplementary investments in accumulators(($\cdot C_{accumulator}$)

The design of accumulators refers to the Boiler and Pressure Vessel Code of American Society of Mechanical Engineers [28]. A typical low alloy steel Q345R is exemplified. As large pressure vessels have a cost in approximate proportion to the vessel weight [29], the material cost of an accumulator is

$$C_{accumulator}=C_{steel}=P_{steel}M_{steel}=P_{steel}\rho_{steel}V_{steel}\times10^{-9} \tag{36}$$

where C_{steel} is the steel cost and P_{steel} is the steel price. A cylinder vessel is commonly adopted and the total volume of steel (V_{steel}) is a function of the inner diameter (D_i), thickness (δ) and height (H) of the vessel.

All the accumulators can be divided into two categories: external and internal pressure vessels. The former is characterized by a higher outer wall pressure than the inner wall pressure, and the latter is the opposite.

3.2.2.1. External pressure vessel. The wall thickness of the cylinder δ_{cy} is [30].

$$p_{cr}\approx2.2E\left(\frac{\delta_{cy}}{D_o}\right)^3 \tag{37}$$

where *E* is the elasticity modulus. D_o is the outer diameter. p_{cr} is the critical pressure and the relationship between p_{cr} and the design pressure *p* is [31].

$$p\le\frac{p_{cr}}{3} \tag{38}$$

The length of the cylinder L_{cy} can be figured out by the vessel volume

$$V_{steel} = \frac{M_{oil} \cdot 1000}{\rho_{@T_{LTA}}} = \pi (D_o - 2\delta_{cy})^2 \cdot L_{cy} \cdot 10^{-6} \tag{39}$$

A cylinder vessel generally has two elliptical heads at the top and the bottom. The standard ratio of the half-long axis to the half-short axis of an ellipse is 2:1. The thickness of the head δ_{head} is regulated by [32].

$$\delta_{head} = 3.46 R_o \sqrt{\frac{p}{E}} \tag{40}$$

where R_0 is the equivalent outer radius of the spherical shell. For a standard ellipsoidal head, $R_0 = 0.9D_0$.

The material mass used for the elliptical head is defined as [33].

$$M_{head} = \rho_{steel} \pi \delta_{head} \left[\frac{D_i^2}{3} + \frac{5}{6} D_i \delta_{head} + \frac{2}{3} \delta_{head}^2 + (D_i + \delta_{head}) h_{head} \right] \cdot 10^{-9} \tag{41}$$

where h_{head} is the edge height of the head (mm) and is regulated by the standard [34].

The material mass required for the cylinder is [33].

$$M_{cy} = \pi \delta_{cy} (D_i + \delta_{cy}) L_{cy} \rho_{steel} \cdot 10^{-9} \tag{42}$$

The total material mass for the vessel is

$$M_{steel} = M_{cy} + 2M_{head} \tag{43}$$

3.2.2.2. Internal pressure vessel. δ_{cy} of an internal pressure vessel is also correlated with p [35].

$$\delta_{cy} = \frac{pD_i}{2[\sigma]^t \varnothing - p} \tag{44}$$

where $\varnothing$ is the welding coefficient. $[\sigma]^t$ is the permissible stress, as posted in Table 2.

δ_{head} is expressed by

$$\delta_{head} = \frac{pD_i}{2[\sigma]^t \varnothing - 0.5p} \tag{45}$$

p is the sum of the saturation pressure of water at the design temperature (p_s) and the static pressure caused by gravity (p_g). The accumulator can be laid in a vertical or horizontal way. But the horizontal layout in Fig. 5 appears to save more material of steel

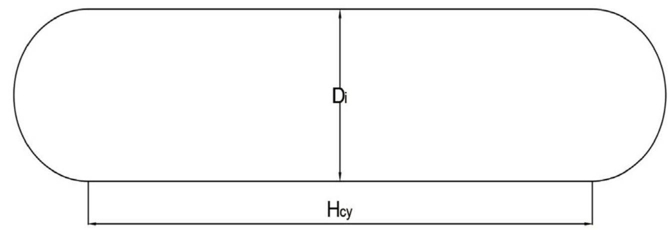

Fig. 5. Horizontal placement of cylinder accumulator.

[33]. p for the horizontal disposition is

$$p = p_s + p_g = p_s + \rho_w g D_i \cdot 10^{-9} \tag{46}$$

Table 2
Permissible stress for Q345R [33], unit: MPa.

Standard	Thickness (mm)	Temperature (°C)					
		200	250	300	350	400	450
GB 713	3–16	183	167	153	143	125	66
	>16-36	170	157	143	133	125	66
	>36-60	160	147	133	123	117	66
	>60-100	150	137	123	117	110	66
	>100-150	147	133	120	113	107	66
	>150-200	143	130	117	110	103	66

3.2.3. Cost of HX3 (C_{HX3})

The purchased cost of HX is [36].

$$log_{10} C_p = K_1 + K_2 log_{10} S + K_3 (log_{10} S)^2 \tag{47}$$

where C_p is a basic cost concerning with the HX area S. Considering the specific material of the construction and operating pressure, the bare module cost for HX should be corrected as [36].

$$C_{BM} = C_P (B_1 + B_2 F_M F_P) \tag{48}$$

C_{BM} is the corrected cost, F_M is the material correction factor, and F_P is a measure that reflects the pressure factor, which is appraised by [36].

$$\log_{10} F_p = C_1 + C_2 \log_{10}(10p - 1) + C_3 [\log_{10}(10p - 1)]^2 \tag{49}$$

K_1, K_2, K_3, B_1, B_2, C_1, C_2 and C_3 are coefficients for the cost evaluation of components. The values are listed in Table 3. Since the unit in the parentheses of the second term in the right-hand side of Eq. (49) is gage pressure in bar, a transformation from MPa to bar is thus needed to fit the equation request.

The actual cost of 2018 needs to be converted from that of 2001 by introducing the Chemical Engineering Plant Cost Index (*CEPCI*) [38].

$$C_{HX3} = C_{BM,\,2018} = C_{BM,\,2001} \cdot CEPCI_{2018} / CEPCI_{2001} \tag{50}$$

where $CEPCI_{2001} = 397$, $CEPCI_{2018} = 648.7$.

3.2.4. Cost of oil (C_{oil})

C_{oil} is 2.2 \$/kg [39,40].

3.2.5. Excess annual yield (Y)

Y_{DVG} is individually expressed by

$$Y_{DVG,\,rated} = P_e \cdot W_{DVG,\,rated} = P_e \cdot \eta_{SORC} \cdot \sum_1^{8760} \left(\eta_{PTC} \cdot I_{DN} \cdot A_{DVG,\,rated} \right) \tag{51}$$

Table 3
Values of constants [37].

Coefficient	K_1	K_2	K_3	C_1	C_2	C_3	B_1	B_2	F_M
Value	4.3247	−0.3030	0.1634	0.0388	−0.11272	0.08183	1.63	1.66	1.40

$$Y_{DVG,\ d} = P_e \cdot W_{DVG,\ d} = P_e \cdot t_{ORC} \cdot \dot{w}_{ORC,d} \cdot 365 \tag{52}$$

where P_e is the electricity price. $W_{DVG,\ SORC}$ is the annual electricity output in Mode 1. η_{SORC} is the SORC efficiency corresponding to the optimum η_{eq} ($\eta_{eq,opt}$). The meaning of $\eta_{eq,opt}$ will be explained in Section 4.1. η_{PTC} is the hourly PTC efficiency in a typical meteorological year. Given the quality of stored oil, $Y_{DVG,\ d}$ remains constant for different areas.

4. Results and discussion

Higher main steam inlet temperature and pressure lead to a higher heat-to-power conversion efficiency but greater technical challenges and more investment cost of steam turbines. The power blocks of the current PTC plants using thermal oils have main steam temperature and pressure of 380 °C/10 MPa (the correlated water evaporation temperature is 311 °C) and the major turbine manufacturers are Siemens and Man-Turbo [1,8]. In light of this, the inlet steam pressure (p_1) and temperature (T_1) are selected as 10 MPa and 311 °C respectively. Other specific parameters are posted in Table 4. Besides, the following assumptions are made. Saturated steam/vapor is assumed at the turbine inlets. Only subcritical cycles are considered. The oil in both HTA and LTA is at the saturated state of vapor-liquid coexistence. The mass of stored oil/water (M_{oil}/ M_w) is divided into three levels: 1000, 1500 and 2000 tonnes. Four widely investigated and adopted fluids are selected: benzene [3,5,6], toluene [5,45,46], cyclohexane [5,47,48] and hexamethyldisiloxane (MM) [5,49,50].

4.1. Performance of the DVG-SORC system

Variations of the top and bottom cycle efficiencies, steam turbine exhaust wetness (y_2) and isentropic efficiency (ε_{ST}) in Mode 1 are graphed in Figs. 6 and 7. η_{SRC} decreases linearly while η_{ORC} rises monotonically with the increment of steam condensation

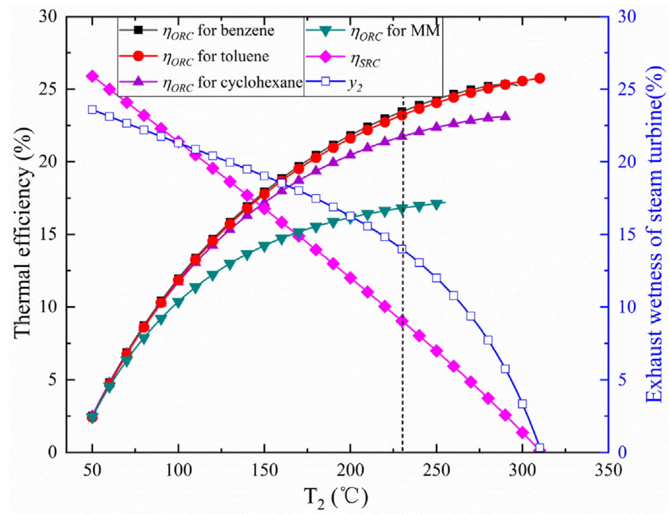

Fig. 6. Variation of steam turbine exhaust wetness, ORC and SRC efficiencies.

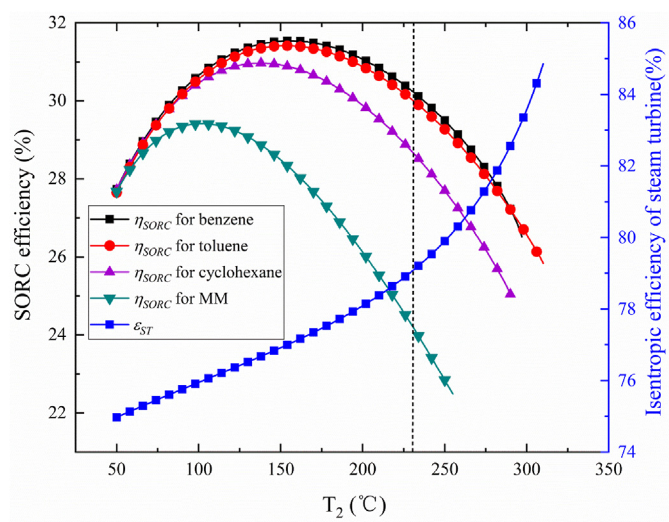

Fig. 7. Efficiencies of SORC and steam turbine.

temperature (T_2). In contrast, η_{SORC} exhibits parabolic variation. $\eta_{SORC,max}$ is 31.54%, 31.41%, 30.97% and 29.42% for benzene, toluene, cyclohexane and MM. Higher T_2 is more favorable to steam turbine performance because y_2 falls down and ε_{ST} increases as T_2 elevates. The reference superheated steam turbine efficiency ($\varepsilon_{ST,sh}$) of 85% is achieved when $y_2 = 0$ (The corresponding T_2 is 311 °C). Generally, y_2 should not be higher than 14% to ensure the reliable operation of wet steam turbines [6,51]. The two dot dash lines denote y_2 of 14%, which correspond to T_2 of 230 °C and ε_{ST} of 79.05%. Bearing this in mind, $\eta_{SORC,max}$ might be impractical and only the data in the right parts of the dotted lines is reasonable.

Discharge duration (t_{ORC}) at variable mass of stored oil (M_{oil}) is presented in Fig. 8. Similar to those in Fig. 7, peak values of t_{ORC} fall on the left half of the dotted line and are not preferable. Given T_2 of

Table 4
Specific parameters for calculation.

Term	Value
Rated power output of SORC, W_{net} [3]	10 MW
Reference efficiency of superheated steam turbine, $\varepsilon_{ST,sh}$ [6]	0.85
Inlet pressure of steam turbine, p_1 [1,8]	10 MPa
Baumann factor, a [26]	1
ORC turbine efficiency, ε_{OT} [5,6]	0.85
Pump efficiency, ε_P [5,6]	0.8
Generator efficiency, ε_g [3,5,6]	0.95
Runtime of SORC (i.e., duration time of radiation), t_{SORC} [5,6]	8 h
Wind speed, v_w [3,5,6]	5 m/s
Standard direct normal solar irradiation, $I_{DN,\ st}$ [3]	0.8 kW/m^2
Ambient temperature, T_a [5,6]	20 °C
ORC condensation temperature, T_{14} [5,6]	30 °C
Minimum temperature difference, ΔT_{min} [3,5,6]	10 °C
Density of steel, ρ_{steel} [41]	7850 kg/m^3
Elasticity modulus for Q345R, E [41]	206 × 10^3 MPa
Edge height of head, h_{head} [34]	25 mm
Welding coefficient, ∅ [33]	0.8
Price of PTC, P_{PTC} [3,42]	170 $/m^2
Price of steel, P_{steel} [3,43]	0.576 $/kg
Price of electricity, P_e [3,44]	0.184 $/kWh

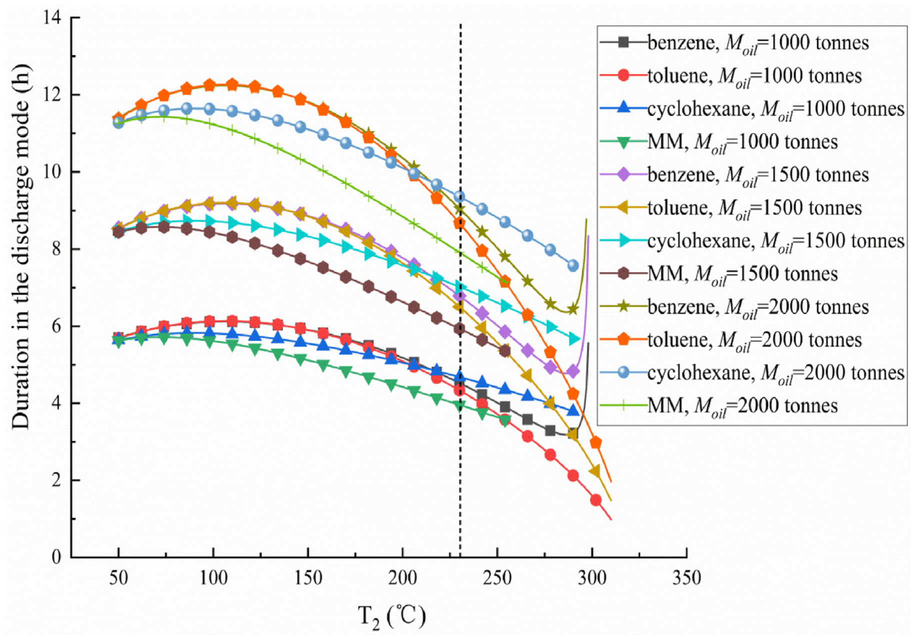

Fig. 8. Discharge duration at different M_{oil}.

230 °C, t_{ORC} ranges from approximately 4 h–10 h when M_{oil} is between 1000 tonnes and 2000 tonnes. Given M_{oil} and $T_2 \geq 230$ °C, the longest t_{ORC} is obtained with cyclohexane, followed by benzene and toluene.

Particularly, the three curves with benzene have steep increments near 300 °C. The reason is that the latent heat $(h_{11} - h_{11,l})$ of benzene decreases sharply when approaching its critical temperature of 288.87 °C. For instance, $(h_{11} - h_{11,l})$ drops from 60.35 kJ/kg to 44.81 kJ/kg when the ORC evaporation temperature (T_{11}) climbs from 287 °C to 288 °C (the related T_2 increases from 297 °C to 298 °C). While the increase in m_{ORC} and $h_{oil,pinch}$ is respectively 1.03 kg/s and 2.17 kJ/kg, which is limited. Meanwhile, T_{HTA} is 321 °C in view of the ΔT_{min} in HTA. Given h_5 of 161.69 kJ/kg, $\dot{m}_{oil}$ declines noticeably according to Eq (14). t_{ORC} is inversely proportional to $\dot{m}_{oil}$ when M_{oil} is constant according to Eq (26). Therefore, t_{ORC} rises dramatically.

The equivalent heat-to-power efficiency (η_{eq}) at different M_{oil} is illustrated in Fig. 9. Less M_{oil} corresponds to smaller storage capacity (t_{ORC}) but higher η_{eq}. The reasons are as follows: as t_{SORC} is fixed at 8 h and ORC efficiency during discharge $(\eta_{ORC,d})$ is lower than η_{SORC}, η_{SORC} is dominant in η_{eq} when $t_{ORC} < t_{SORC}$. It can be inferred that η_{eq} equals η_{SORC} when $t_{ORC} = 0$ and η_{eq} equals $\eta_{ORC,d}$ when $t_{ORC} = \infty$. Given M_{oil}, η_{eq} for benzene is marginally higher

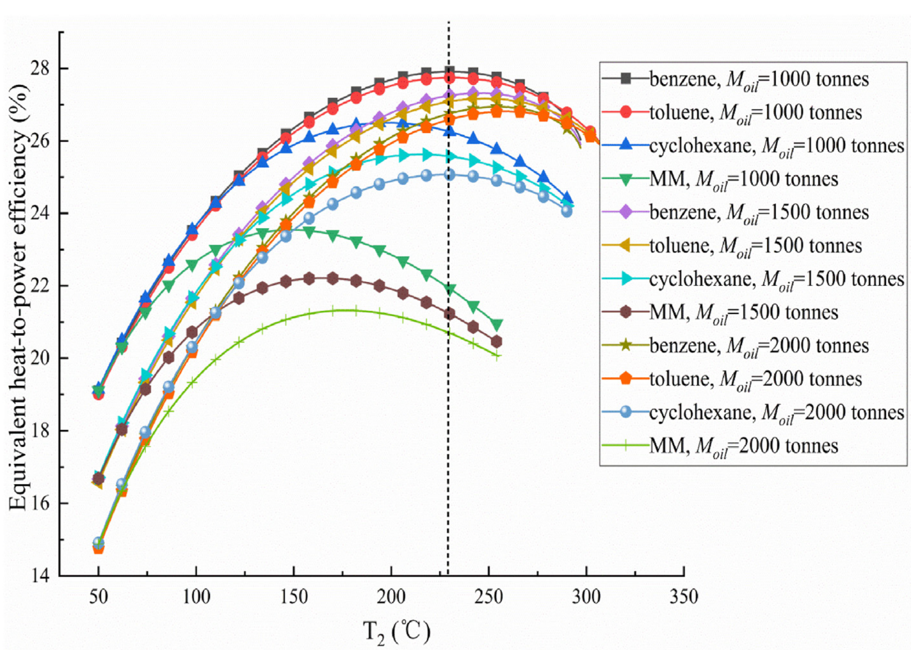

Fig. 9. Equivalent heat-to-power efficiency at different M_{oil}.

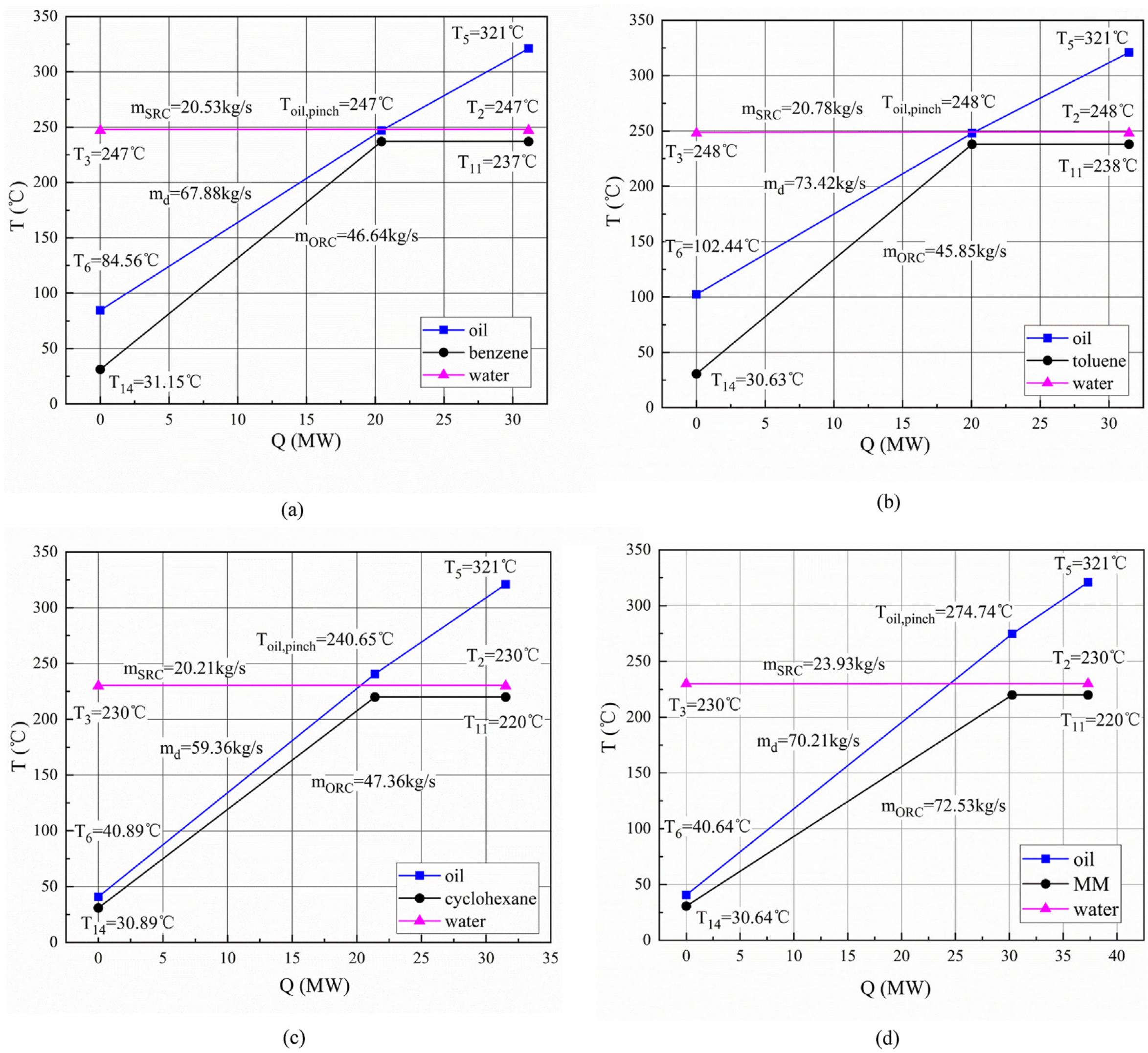

Fig. 10. Heat transfer during Modes 1 and 2 for different ORC fluids when M_{oil} = 1500 tonnes: (a) benzene; (b) toluene; (c) cyclohexane; (d) MM.

than that for toluene, and they are appreciably higher than those with cyclohexane and MM.

Notably, T_2 corresponding to $\eta_{eq,max}$ ($T_{2,max}$) falls in the right part of the dotted line for benzene and toluene, which is contrary to the results for the remaining two fluids. The optimum η_{eq} ($\eta_{eq,opt}$) is defined as the peak η_{eq} taking into account the constraint that $y_2 \leq$ 14%. $\eta_{eq,opt} = \eta_{eq,max}$ for benzene and toluene, while $\eta_{eq,opt} < \eta_{eq,max}$ for cyclohexane and MM.

The heat transfer characteristics in HX2 and HX3 at $\eta_{eq,opt}$ are exhibited in Fig. 10. M_{oil} of 1500 tonnes is exemplified. The evaporator for the bottom ORC is HX2 in Mode 1 and it is switched to HX3 during Mode 2. Since the thermodynamic parameters and mass flow rate of the bottom ORC stay unchanged, the *T-Q* curves of the four fluids remain constant in various modes. In particular, the minimum temperature difference (δT_{min}) takes place at the pinch point for benzene and toluene, while it occurs at the ORC fluid inlet for cyclohexane and MM in HX3.

4.2. Thermodynamic performance comparison with the DSG-SORC system

Design parameters corresponding to $\eta_{eq,opt}$ are displayed in Table 5. The maximum $\eta_{eq,opt}$ is 27.91% for benzene at M_{oil} = 1000 tonnes and the minimum is 20.69% for MM at M_{oil} = 2000 tonnes. As explained previously, T_2 for $\eta_{eq,opt}$ ($T_{2,opt}$) exceeds 230 °C for benzene and toluene, while $T_{2,opt}$ = 230 °C for cyclohexane and MM. The LTA temperature (T_{LTA}) with benzene and toluene as the ORC fluid is considerably higher than that with cyclohexane and MM. The reason can be illustrated by the location of ΔT_{min} in Fig. 10, and simultaneously $T_{LTA} = T_6$.

The related parameters for the DSG-SORC system are listed in Table 6. The mainstream inlet temperature and HTA temperature are 270 °C. Other device efficiencies and fixed parameters are the same as those listed in Table 4. $\eta_{eq,opt}$ varies from 18.54% to 25.75% for the DSG-SORC system. The relative improvement of $\eta_{eq,opt}$ is 7.72–11.60% by replacing water with oil as the heat carrier and storage fluid. The remaining indicators (η_{SORC}, η_{ORC}, $\eta_{ORC,d}$ and η_{SRC}) are elevated appreciably except for MM. It is worth noting that y_2 is less than 14% for the four fluids, which manifests $\eta_{eq,opt} = \eta_{eq,max}$ and $T_{2,opt} = T_{2,max}$ in the case of DSG-SORC.

Compared with the DSG solution, T_{LTA} in the DVG scheme is dramatically reduced by 66–104 °C except for MM. Given T_{HTA} of 321 °C, the temperature drop between the two accumulators reaches 200–280 °C (117–155 °C greater than that of the DSG type). A

Table 5
Design parameters corresponding to $\eta_{eq,opt}$ when $y_2 \leq 14\%$ for the DVG-SORC system.

ORC fluids	M_{oil} (tonne)	$\eta_{eq,opt}$ (%)	η_{SORC} (%)	η_{ORC} (%)	$\eta_{ORC,d}$ (%)	η_{SRC} (%)	$T_{2,opt}$ (°C)	y_2 (%)	T_{LTA} (°C)	t_{ORC} (h)
Benzene	1000	27.91	30.25	23.50	23.42	8.94	231	13.90	67.81	4.50
	1500	27.32	29.63	24.19	24.07	7.30	247	12.33	84.56	6.14
	2000	26.94	29.19	24.56	24.42	6.25	257	11.17	95.42	7.65
Toluene	1000	27.75	29.97	23.31	23.17	8.84	232	13.81	80.50	4.28
	1500	27.17	29.36	23.99	23.84	7.20	248	12.22	102.44	5.67
	2000	26.82	28.83	24.43	24.26	5.93	260	10.79	122.19	6.74
Cyclo	1000	26.26	28.70	21.74	21.63	9.04	230	13.99	40.89	4.68
-hexane	1500	25.57	28.70	21.74	21.63	9.04	230	13.99	40.89	7.02
	2000	25.07	28.70	21.74	21.63	9.04	230	13.99	40.89	9.36
	1000	21.92	24.25	16.81	16.72	9.04	230	13.99	40.64	3.96
MM	1500	21.23	24.25	16.81	16.72	9.04	230	13.99	40.64	5.93
	2000	20.69	24.25	16.81	16.72	9.04	230	13.99	40.64	7.91

Table 6
Design parameters corresponding to $\eta_{eq,opt}$ when $y_2 \leq 14\%$ for the DSG-SORC system.

ORC fluids	M_w (tonne)	$\eta_{eq,opt}$ (%)	η_{SORC} (%)	η_{ORC} (%)	$\eta_{ORC,d}$ (%)	η_{SRC} (%)	$T_{2,opt}$ (°C)	y_2 (%)	T_{LTA} (°C)	t_{ORC} (h)
Benzene	1000	25.75	27.55	23.41	21.99	5.49	229	6.70	161.06	4.08
	1500	25.26	27.02	23.86	22.25	4.22	239	5.34	181.26	4.88
	2000	25.01	26.56	24.19	22.48	3.17	247	4.19	199.79	5.07
	1000	25.55	27.42	23.07	21.65	5.74	227	6.95	161.17	4.07
Toluene	1500	25.07	26.74	23.66	21.96	4.10	240	5.23	187.93	4.48
	2000	24.77	26.26	23.99	22.06	3.05	248	4.03	206.81	4.53
Cyclo -hexane	1000	24.10	26.87	21.07	20.05	7.45	213	8.55	106.93	5.94
	1500	23.47	26.06	21.63	20.46	5.74	227	6.95	130.90	7.30
	2000	23.09	25.75	21.81	20.56	5.12	232	6.32	141.11	8.89
	1000	20.33	26.09	14.78	14.05	13.40	161	13.13	40.18	8.54
MM	1500	19.21	25.05	15.51	14.78	11.40	179	11.73	40.26	12.00
	2000	18.54	24.19	15.94	15.21	9.92	192	10.61	40.33	15.18

larger temperature difference is desirable for improving the storage capacity. Besides, T_{LTA} on the use of cyclohexane in Table 6 far exceeds the ORC fluid inlet temperature of 30.8 °C. For the DSG-SORC, ΔT_{min} usually occurs at the fluid's pinch point. Finally, t_{ORC} is extended by 0.42–2.58 h for benzene and 0.21–2.21 h for toluene. A larger mass of storage medium leads to a more appreciable extension. But t_{ORC} is shortened by 0.28–7.27 h for cyclohexane and MM. It indicates that the DVG has an adverse effect on the SORC storage capacity by using these two fluids.

4.3. Thermo-economic performance comparison between the two systems

In this section, benzene is employed as the ORC fluid in both systems. The design parameters in accordance with $\eta_{eq,opt}$ when the stored mass is 1500 and 2000 tonnes are exemplified.

4.3.1. Cost of the accumulators

Take the LTA at $M_{oil} = 1500$ tonnes as an instance. It is an external pressure vessel. Variations of total mass of steel (M_{steel}), length of the cylinder (L_{cy}), and length-diameter ratio with the outer diameter (D_o) are depicted in Fig. 11. L_{cy} could be extremely high at low D_o. There will be great difficulty in fabricating and transporting such a vessel. Since the volume of stored oil is constant, the consumed weight of steel varies moderately due to the slight mass change in the elliptical head. Considering the simplicity of manufacturing and transportation, L_{cy} of 25–35 m and length-diameter ratio of 2–6 are constrained. Finally, D_o of 8000 mm is determined and the relevant parameters are indexed in Table 7. The data for δ_{cy} and δ_{head} are rounded off.

The LTA at $M_{oil} = 2000$ tonnes is also an external pressure vessel and the rest accumulators are internal pressure type. Notably, the volume of HTA will be exceedingly huge if a single vessel is

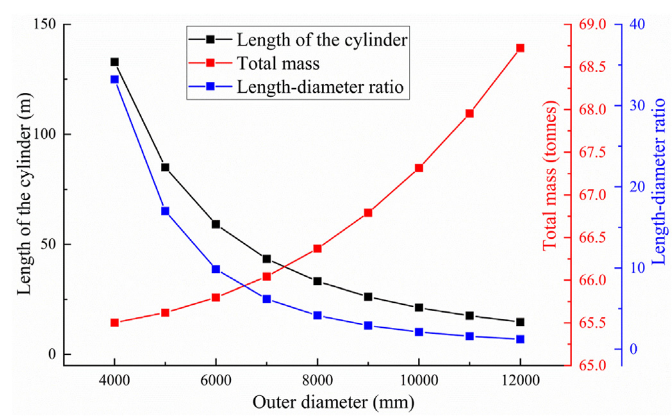

Fig. 11. Variations of M_{steel}, L_{cy} and length-diameter ratio of the LTA with D_o when $M_{oil} = 1500$ tonnes.

employed for $M_w = 1500$ or 2000 tonnes. Two or more vessels in parallel provide an effective solution [33]. The HTA is divided into two containers at $M_w = 1500$ tonnes and three containers at $M_w = 2000$ tonnes. As displayed in the last row, the steel cost (C_{steel}) for the DSG system dramatically exceeds (78.7 times at 1500 tonnes and 72.4 times at 2000 tonnes) that of the DVG system.

4.3.2. Cost of HX3

The HX cost is mainly related to its area and amount of materials in use [7,52]. The investigated HX3 is a single shell and double tube pass HX. Shell and tube HXs have advantages of great flexibility, high operating pressure/temperature, great availability, high value of heat transfer and low costs [7,53]. The hot fluid is located in shell side and the cold fluid is in tube side. A tube outer diameter of 19 mm and a tube pitch of 25 mm are adopted, which are common

Table 7
Design parameters of the accumulators.

Accumulators	DVG-SORC system				DSG-SORC system			
	M_{oil} = 1500 tonnes		M_{oil} = 2000 tonnes		M_w = 1500 tonnes		M_w = 2000 tonnes	
Parameters	HTA	LTA	HTA	LTA	HTA	LTA	HTA	LTA
$\boldsymbol{p}$ **(kPa)**	486	0.294	498	0.544	5548	1102	5548	1719
D_o **(mm)**	10,043	8000	12,052	10,000	6367	8083	6367	10,176
$\boldsymbol{\delta_{cy}}$ **(mm)**	21	10	26	15	183	42	183	88
$\boldsymbol{L_{cy}}$ **(m)**	33.66	33.23	31.16	28.65	34.56	33.69	30.72	28.75
Length-diameter ratio	3.35	4.15	2.59	2.86	5.43	4.17	4.83	2.83
$\boldsymbol{D_i}$ **(mm)**	10,000	7980	12,000	9969	6000	8000	6000	10,000
$\boldsymbol{V_{steel,\ cy}}$ **($\mathbf{m^3}$)**	22.57	8.33	30.78	13.78	123.04	35.44	109.37	80.30
$\boldsymbol{\delta_{head}}$ **(mm)**	21	1	26	2	181	42	181	88
$\boldsymbol{M_{head}}$ **(tonne)**	17.72	0.50	31.28	1.32	58.22	22.34	58.22	74.26
$\boldsymbol{M_{steel,\ cy}}$ **(tonne)**	177.19	65.38	241.68	108.16	965.85	278.18	858.57	620.33
$\boldsymbol{M_{steel}}$ **(tonne)**	212.63	66.37	304.25	110.79	1082.28	322.86	975.01	778.84
$\boldsymbol{C_{steel}}$ **($\times 10^4$ \$)**	12.25	3.82	17.52	6.38	1246.79	18.60	1684.82	44.86

in industrial production. Over design area of approximately 5–10% is ensured.

HTRI software, which is considered to be the industry's most advanced thermal process design and simulation software [54], is used to estimate the HX3 area. The physical parameters of the oil can be derived from Aspen Plus [55] by importing mass fraction of 26.5% bipheny and 73.5% diphenyl oxide. Then the parameters like density, heat capacity, thermal conductivity and viscosity can be imported from Aspen Plus into HTRI. The calculation procedure of the required area (S) in HTRI is given in the authors' previous work [7]. The scheme of HX3 is graphed in Fig. 12 and the design parameters are provided in Table 8.

4.3.3. Equivalent payback period (EPP)

The standard direct normal solar irradiance ($I_{DN,\ st}$) is 0.8 kW/m^2, and is perpendicular to the collector aperture. The standard wind speed ($v_{W,\ st}$) is 5 m/s. The standard sunshine duration ($t_{s,\ st}$) is 8.373, 6.890, 6.392, 5.534, 7.649 and 4.729 h for Phoenix,

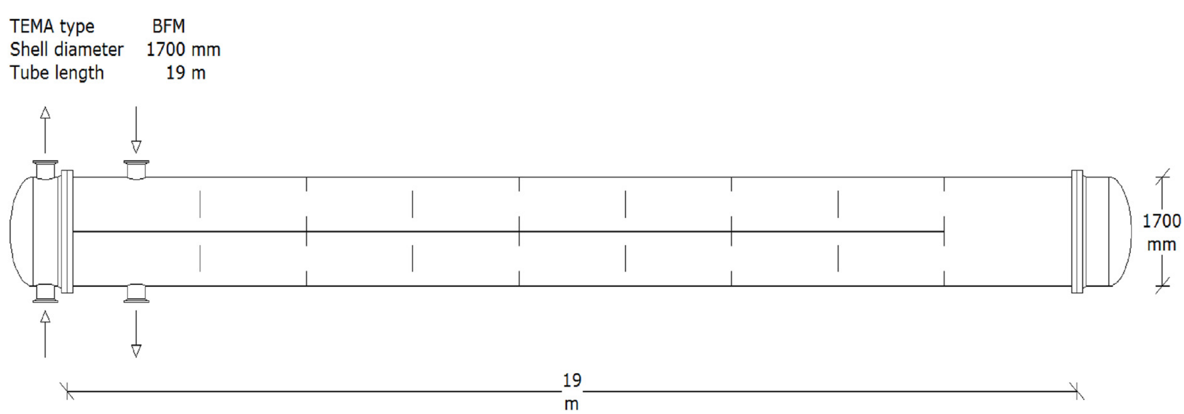

(a)

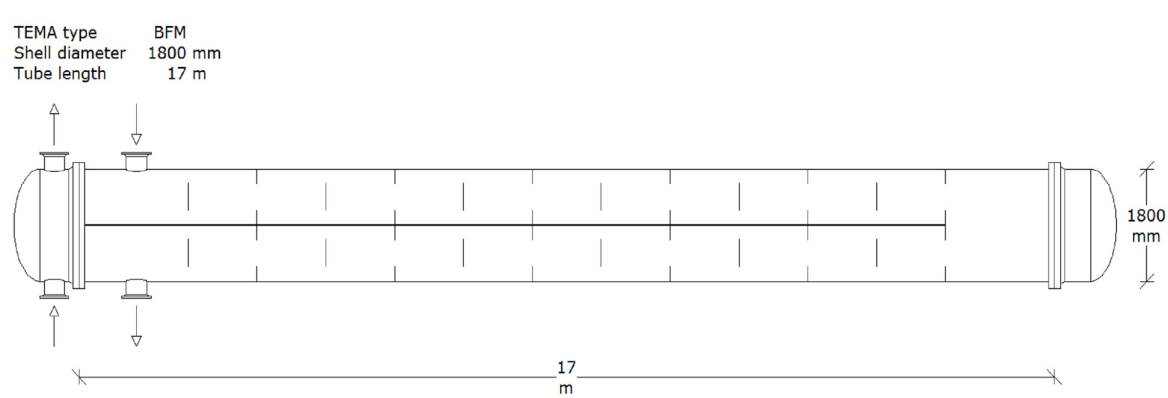

(b)

Fig. 12. Scheme of HX3 for (a) M_{oil} = 1500 tonnes; (b) M_{oil} = 2000 tonnes.

Table 8
Design parameters of HX3.

Process data	HX3 (1500/2000 tonnes)
Shell side heat transfer coefficient, kW/m²·K	0.637/0.609
Shell ID, mm	1700/1800
Shell side velocity, m/s	0.11/0.19
Tube side heat transfer coefficient, kW/m²·K	0.701/0.679
Tube length, m	19/17
Tube side velocity, m/s	0.22/0.20
Tube count	5476/6249
Overall heat transfer coefficient, kW/m²·K	0.284/0.274
Heat duty, MW	30.763/31.982
Inlet/Outlet height under nozzles, mm	0/0
Baffle central spacing, mm	2000/1200
Effective mean temperature difference, °C	22.4/23.7
Area, m²	5163.00/5253.17
Over design, %	6.94/6.47
C_{HX3} ($\times 10^4$ $)	183.619/186.540

Table 9
Required PTC area and annual output at $M_{oil} = M_w = 1500$ tonnes.

Region	Phoenix	Sacramento	Cape Town	Canberra	Lhasa	Delingha
$A_{DVG,\ rated}$/ $A_{DSG,\ rated}$ ($\times 10^4$ m²)	5.351/5.891	6.502/7.158	7.010/7.716	8.096/8.912	5.857/6.448	9.475/10.430
$A_{DVG,\ d}$ / $A_{DSG,\ d}$ ($\times 10^4$ m²)	3.777/3.413	4.590/4.147	4.948/4.471	5.715/5.164	4.135/3.736	6.688/6.043
$W_{DVG,\ rated}$ / $W_{DSG,\ rated}$ ($\times 10^4$ kWh/year)	2575.83/2586.68	2558.69/2569.55	2404.47/2414.60	2582.28/2593.47	2249.23/2258.98	2636.55/2648.53

Sacramento, Cape Town, Canberra, Lhasa and Delingha, respectively, based on the typical weather data [56]. The economic indicators for the two scenarios are presented in Tables 9–12. The required PTC area in Mode 1 for the DVG system ($A_{DVG,\ rated}$) is less than that of the DSG system, while the area in Mode 2 ($A_{DVG,\ d}$) exceeds that of the DSG system. Annual power output in the rated mode for the DVG system ($W_{DVG,\ rated}$) is marginally reduced (9.76–11.98 × 10^4 kWh at 1500 tonnes and 5.90–7.16 × 10^4 kWh at 2000 tonnes) by comparison with the DSG configuration. The yearly electricity generated in Mode 2 (W_d) is not listed as it does not change with the location. $W_{DVG,\ d}$ is 1679.59 × 10^4 kWh and 2181.38 × 10^4 kWh when $M_{oil} = 1500$ and 2000 tonnes; $W_{DSG,\ d}$ is 1408.22 × 10^4 kWh and 1463.30 × 10^4 kWh when $M_w = 1500$ and 2000 tonnes. Notably, the supplementary investments in PTCs (ΔC_{PTC}) are negative in Table 10, which indicates the DVG system saves area at 1500 tonnes. *EPP* is generally within 7.5 years at 1500 tonnes and 5 years at 2000 tonnes.

Table 10
ΔC_{PTC}, C_{add}, Y and *EPP* at $M_{oil} = M_w = 1500$ tonnes.

Region	ΔC_{PTC} ($\times 10^4$ $)	C_{add} ($\times 10^4$ $)	Y ($\times 10^4$ $/year)	*EPP* (years)
Phoenix	−29.773	356.641	47.937	7.440
Sacramento	−36.179	350.235	47.933	7.307
Cape Town	−39.001	347.413	48.067	7.228
Canberra	−45.044	341.370	47.873	7.131
Lhasa	−32.589	353.825	48.137	7.351
Delingha	−52.715	333.699	47.728	6.992

5. Comparison with the conventional PTC system using synthetic oils

In the above analysis, a maximum η_{SORC} of 30.25% is achieved at the given p_1 of 10 MPa and T_1 of 311 °C. η_{SORC} can be further improved by elevating p_1 and T_1, and modifying the structure. The modified system is graphed in Fig. 13. p_1 and T_{HTA} are set at 18.6 MPa and 393 °C, which are the same as the input pressure in a boiler power plant [57] and the hot tank temperature in the traditional PTC systems [1]. The saturation temperature of water at 18.6 MPa is about 360 °C. T_{11} and T_{18} are selected as 280 °C and 120 °C, respectively. Toluene is exemplified as the ORC fluid and all the key parameters are indexed in Table 13.

It is figured out that $\varepsilon_{ST} = 80.97\%$, $\eta_{SRC} = 7.09\%$, $\eta_{ORC} = 32.15\%$ and $\eta_{SORC} = 36.82\%$. η_{SORC} is in close proximity to 37.7% that achieved by the conventional PTC systems [1]. But the temperature drop between the two tanks reaches 208 °C, which is magnified by 2.08 times (the storage temperature of the existing plants ranges from 293 °C to 393 °C [1]). Besides, the technical challenges inherent in the low-pressure cylinders in wet steam turbines are omitted. Unlike water, dry organic fluid will enter a superheated state if it expands from a saturated vapor state, thereby offering a safe and efficient expansion process. The ORC turbine is typically a dry turbine with an isentropic efficiency exceeding 90% [58]. There is still large room for efficiency improvement in η_{SORC} by optimizing T_{11} and T_{18}, as well as employing more efficient ORC turbines.

Given the above conditions, the power generation by 1 kg thermal oil in the discharge process is 0.0437 kWh. In comparison, it is only 0.0255 kWh/kg in the discharge process of conventional solar PTC systems. The proposed system has a lower heat-to-power efficiency during discharge (32.15% vs. 37.7%) but a significantly higher temperature drop, leading to a larger storage capacity per mass. It may be able to reduce the payback time of the solar power system owing to the cost reduction potential in the storage unit.

Table 12
ΔC_{PTC}, C_{add}, Y and *EPP* at $M_{oil} = M_w = 2000$ tonnes.

Region	ΔC_{PTC} ($\times 10^4$ $)	C_{add} ($\times 10^4$ $)	Y ($\times 10^4$ $/year)	*EPP* (years)
Phoenix	124.378	561.482	130.810	4.292
Sacramento	151.133	588.237	130.866	4.495
Cape Town	162.923	600.027	131.043	4.579
Canberra	188.168	625.272	130.938	4.775
Lhasa	136.139	573.243	130.924	4.378
Delingha	220.220	657.324	131.023	5.017

Table 11
Required PTC area and annual output at $M_{oil} = M_w = 2000$ tonnes.

Region	Phoenix	Sacramento	Cape Town	Canberra	Lhasa	Delingha
$A_{DVG,\ rated}$/ $A_{DSG,\ rated}$ ($\times 10^4$ m²)	5.435/6.010	6.604/7.303	7.119/7.872	8.222/9.092	5.949/6.578	9.622/10.641
$A_{DVG,\ d}$ / $A_{DSG,\ d}$ ($\times 10^4$ m²)	4.837/3.530	5.877/4.289	6.336/4.624	7.317/5.340	5.294/3.864	8.564/6.250
$W_{DVG,\ SORC}$ / $W_{DSG,\ SORC}$ ($\times 10^4$ kWh/year)	2575.18/2582.35	2557.83/2564.69	2403.37/2409.26	2581.03/2587.50	2248.69/2255.24	2634.63/2640.63

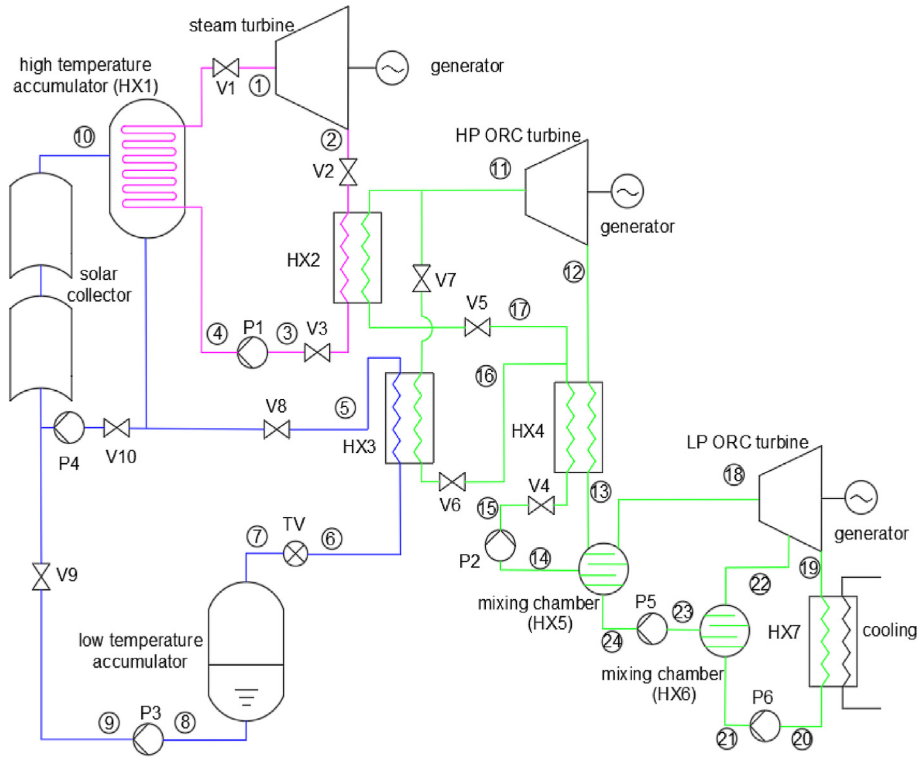

Fig. 13. Modified DVG-SORC system in higher temperature application (>380 °C).

Table 13
Thermodynamic parameters of each state point.

State point	Temperature (°C)	Pressure (MPa)	Enthalpy (kJ/kg)	Quality (%)	Mass flow rate (kg/s)
1	383	18.67	2755.9	superheated	18.79
2	290	7.44	2626.7	90.52	18.79
3	290	7.44	1290	0	18.79
4	295.28	18.67	1310.27	subcooled	18.79
5	393	0.998	782.23	0	52.67
6	184.66	0.998	305.37	subcooled	52.67
7	184.66	0.013	305.37	0	52.67
11	280	2.53	588.44	100	55.67
12	191.51	0.131	491.46	superheated	55.67
13	122.51	0.131	377.33	superheated	55.67
14	120	0.131	19.03	0	55.67
15	121.32	2.53	22.18	subcooled	55.67
16 (17)	174.66	2.53	137.30	subcooled	55.67
18	120	0.131	373.46	0	55.67
19	51.76	0.005	286.17	superheated	38.09
20	30	0.005	−149.69	0	38.09
21	30.06	0.125	−149.50	subcooled	38.09
22	118.83	0.125	371.99	superheated	17.58
23	118.1	0.125	15.16	0	55.67
24	118.1	0.131	15.16	subcooled	55.67

6. Conclusion

The proposed DVG-SORC system has great potential to solve the technical difficulties associated with heat collection and storage inherent in the DSG-SORC and DSG-CORC systems. By replacing water with the synthetic oil Therminol® VP-1, the pressure-bearing problems in both the tanks and the absorber tubes are greatly alleviated on account of the much lower saturation pressure of the oil. The results show that:

(1) η_{eq} balances the electricity outputs in the two operation modes. $\eta_{eq,opt}$ ranges from 20.69% to 27.91%, which is 7.72–11.60% higher than that of the DSG-SORC scheme. η_{SORC}, η_{ORC}, $\eta_{ORC,d}$ and η_{SRC} are improved to varying degrees except for MM. t_{ORC} is elevated by 0.42–2.58 h for benzene and 0.21–2.21 h for toluene, but shortened for cyclohexane and MM.

(2) The temperature difference between the HTA and LTA can reach about 280 °C, which is significantly higher than that of 100 °C in a conventional PTC system. The proposed system can have a higher storage capacity at a given amount of thermal oil.

(3) The thickness of the oil tanks is noticeably thinner than that of the steam accumulators, thus saving the consumption of

steel. $C_{accumulator}$ is less than one-seventieth of the steam tanks. The DVG system saves 29.773–52.715 $\times$ 10^4 \$ in PTC cost at 1500 tonnes but requires additional 124.378–220.220 $\times$ 10^4 \$ for aperture area at 2000 tonnes. The excess annual yield is approximately 48 $\times$ 10^4 \$/year at 1500 tonnes and 131 $\times$ 10^4 \$/year at 2000 tonnes. The corresponding *EPP* is merely within 7.5 years and 5 years for the six territories with abundant beam solar radiation, which implies that the DVG-SORC system seems more cost-effectiveness.

Credit author statement

Pengcheng Li: Writing, Review & Editing; Haiwei Lin: Investigation; Jing Li: Conceptualization, Methodology & Formal analysis; Qing Cao: Writing & Original Draft; Yandong Wang: Software; Gang Pei: Supervision; Desuan Jie: Methodology; Zilong Zhao: Data Curation.

Declaration of competing interest

The authors declare that they have no known competing financial interests or personal relationships that could have appeared to influence the work reported in this paper.

Data availability

Data will be made available on request.

Acknowledgment

This study was sponsored by the Anhui Provincial Natural Science Foundation (2008085QE235, 2008085QE224), the Fundamental Research Funds for the Central Universities (JZ2022HGTB0266, JZ2022HGTB0241), DONGFANG ELECTRIC Dongfang Boiler Group CO., LTD., Postdoctoral Research Project of Sichuan Province and Youth Fund of National Natural Science Foundation of China (JZ2021GJQN0389).

References

[1] González-Roubaud E, Pérez-Osorio D, Prieto C. Review of commercial thermal energy storage in concentrated solar power plants: steam vs. molten salts. Renew Sustain Energy Rev 2017;80:133–48.
[2] Casati E, Galli A, Colonna P. Thermal energy storage for solar-powered organic Rankine cycle engines. Sol Energy 2013;96:205–19.
[3] Li J, Gao GT, Kutlu C, Liu KL, Pei G, SuYH, et al. A novel approach to thermal storage of direct steam generation solar power systems through two-step heat discharge. Appl Energy 2019;236:81–100.
[4] Li J, Gao GT, Pei G, Li PC, SuYH, Ji J, et al. A novel concentrated solar power system using cascade steam-organic Rankine cycle and two-stage accumulators. Energy Proc 2017;142:386–94.
[5] Gao GT, Li J, Li PC, Yang HL, Pei G, Ji J. Design and analysis of an innovative concentrated solar power system using cascade organic Rankine cycle and two-tank water/steam storage. Energy Convers Manag 2021;237:114108.
[6] Gao GT, Li J, Li PC, Cao JY, Pei G, Dabwan YN, et al. Design of steam condensation temperature for an innovative solar thermal power generation system using cascade Rankine cycle and two-stage accumulators. Energy Convers Manag 2019;184:389–401.
[7] Li PC, Cao Q, Li J, Wang YD, Pei G, Gao C, et al. Effect of regenerator on the direct steam generation solar power system characterized by prolonged thermal storage and stable power conversion. Renew Energy 2020;159:1099–116.
[8] NREL. Concentrating solar power projects. Parabolic Trough Projects. https://solarpaces.nrel.gov/by-technology/parabolic-trough. [Accessed 26 May 2022].
[9] Yang HL, Wang QL, Huang YH, Gao GT, Feng JS, Li J, et al. Novel parabolic trough power system integrating direct steam generation and molten salt systems: preliminary thermodynamic study. Energy Convers Manag 2019;195:909–26.
[10] SUN2HEAT® Solutions. Sun & Glass. A Strategic Alliance 2018. https://www.rioglass.com/rioglass-sun-2-heat-solutions/. [Accessed 30 September 2021].
[11] RTUVR® Solar Vacuum Receivers. RTUVR® 70M4 2019. http://en.royalcsp.com/index.php?m=content&c=index&a=lists&catid=15. [Accessed 30 September 2021]. accessed.
[12] Krüger D, Krüger J, Pandian Y, O'Connell B, Feldhoff JF, Karthikeyan R, et al. In: Experiences with direct steam generation at the Kanchanaburi solar thermal power plant. 18th SolarPACES conference; 2012. Marrakech, Morocco.
[13] Wendt DS, Mines GL, Turchi CS, Zhu GD, Cohan S, Angelini L, et al. Stillwater hybrid geo-solar power plant optimization analyses. GRC Trans 2015;39.
[14] Manente G. Analysis and development of innovative binary cycle power plants for geothermal and combined geo-solar thermal resources. In: Doctoral Dissertation of Università degli Studi di Padova; 2011.
[15] Zarza E, Rojas ME, González L, Caballero JM, Rueda F. INDITEP: the first pre-commercial DSG solar power plant. Sol Energy 2006;80:1270–6.
[16] The DISS project: direct steam generation in parabolic trough systems. Operation and maintenance experience. Update on project status, https://p2infohouse.org/ref/46/45473.pdf. [Accessed 19 January 2022].
[17] Eastman Corp. https://www.eastman.com/Literature_Center/T/TF9141.pdf. [Accessed 19 January 2022].
[18] Giostri A, Binotti M, Astolfi M, Silva P, Macchi E, Manzolini G. Comparison of different solar plants based on parabolic trough technology. Sol Energy 2012;86:1208–21.
[19] Therminol VP-1 heat transfer fluid product description. https://www.therminol.com/product/71093459?pn=Therminol-VP-1-Heat-Transfer-Fluid. [Accessed 19 January 2022].
[20] Li S, Ma HJ, Li WY. Dynamic performance analysis of solar organic Rankine cycle with thermal energy storage. Appl Therm Eng 2018;129:155–64.
[21] Casati E, Desideri A, Casella F, Colonna P. Preliminary assessment of a novel small CSP plant based on linear collectors, ORC and direct thermal storage. In: Proceedings Solar PACES; 2012.
[22] Sinasac Z, Jianu OA. Parametric study on the exergetic and cyclic performance of a solar-powered organic Rankine cycle coupled with a thermal energy storage and complete flashing cycle. Sustain Energy Techn 2021;45:101172.
[23] Shu GQ, Zhao MR, Tian H, Wei HQ, Liang XY, Huo YZ, et al. Experimental investigation on thermal OS/ORC (Oil Storage/Organic Rankine Cycle) system for waste heat recovery from diesel engine. Energy 2016;107:693–706.
[24] NREL. System. Advisor Model 2018. http://sam.nrel.gov. [Accessed 19 January 2022].
[25] Leyzerovich A. Wet-steam turbines for nuclear power plants. American ed. PennWell Corp; 2015.
[26] Petr V, Kolovratnik M. Wet steam energy loss and related Baumann rule in low pressure steam turbines. Proc Inst Mech Eng Part A-J Power Energy 2014;228:206–15.
[27] Li J, Alvi JZ, Pei G, Su YH, Li PC, Gao GT, et al. Modelling of organic Rankine cycle efficiency with respect to the equivalent hot side temperature. Energy 2016;115:668–83.
[28] ASME. ASME boiler & pressure vessel code case 2642. New York: American Society of Engineers; 2010. 2010 Mechanical Engineers.
[29] Vessel cost estimate. http://matche.com/equipcost/Vessel.html. [Accessed 30 September 2021].
[30] Lin YJ. Fundamentals of pressure vessel design. China Petrochemical Press; 2016. p. 130 [Chapter 4].
[31] Pressure vessels. National standard of the People's Republic of China. GB/T 150-2011.
[32] Lin YJ. Fundamentals of pressure vessel design. China Petrochemical Press; 2016. p. 154 [Chapter 4].
[33] Li J, Li PC, Gao GT, Pei G, Su YH, Ji J. Thermodynamic and economic investigation of a screw expander-based direct steam generation solar cascade Rankine cycle system using water as thermal storage fluid. Appl Energy 2017;195:137–51.
[34] Elliptical heads. Standards of the machinery department of the People's Republic of China, JB1154-J1173.
[35] Steel pressure vessels. National Standard of the People's Republic of China. GB 150-1998. pp. 28.
[36] Zhang C, Liu C, Wang SK, Xu XX, Li QB. Thermo-economic comparison of subcritical organic Rankine cycle based on different heat exchanger configurations. Energy 2017;123:728–41.
[37] Li J, Hu SZ, Yang FB, Duan YY, Yang Z. Thermo-economic performance evaluation of emerging liquid-separated condensation method in single-pressure and dual-pressure evaporation organic Rankine cycle systems. Appl Energy 2019;256:113974.
[38] Turton R, Bailie RC, Whiting WB, Shaeiwit JA, Bhattacharyya D. Analysis, synthesis, and design of chemical processes. Pearson Education Inc; 2009.
[39] Gil A, Medrano M, Martorell I, Lázaro A, Dolado P, Zalba B, et al. State of the art on high temperature thermal energy storage for power generation. Part 1—Concepts, materials and modellization. Renew Sustain Energy Rev 2010;14:31–55.
[40] Chacartegui R, Vigna L, Becerra JA, Verda V. Analysis of two heat storage integrations for an Organic Rankine Cycle Parabolic trough solar power plant. Energy Convers Manag 2016;125:353–67.
[41] Design code for steel structures. National Standard of the People's Republic of China. GB50017-2003. pp. 29.
[42] Kurup P, Turchi CS. Parabolic trough collector cost update for the system advisor model (SAM). 2015. NREL/TP-6A20-65228.
[43] FOB prices of steel products. Shanghai Ganglian E-Commerce Co., Ltd.; 2017. https://www.mysteel.net/. [Accessed 19 January 2022].

[44] Red document: the first batch of solar thermal power generation demonstration project electricity price will not be regressive! Unified 1.15 ¥/kWh. 2021. http://www.cspplaza.com/article-20207-1.html. [Accessed 19 January 2022].
[45] Linnemann M, Priebe KP, Heim A, Wolff C, Vrabec J. Experimental investigation of a cascaded organic Rankine cycle plant for the utilization of waste heat at high and low temperature levels. Energy Convers Manag 2020;205:112381.
[46] Herrera-Orozco I, Valencia-Ochoa G, Duarte-Forero J. Exergo-environmental assessment and multi-objective optimization of waste heat recovery systems based on Organic Rankine cycle configurations. J Clean Prod 2021;288:125679.
[47] Abbas WKA, Vrabec J. Cascaded dual-loop organic Rankine cycle with alkanes and low global warming potential refrigerants as working fluids. Energy Convers Manag 2021;249:114843.
[48] Liang Z, Liang YZ, Luo XL, Chen JY, Yang Z, Wang C, et al. Superstructure-based mixed-integer nonlinear programming framework for hybrid heat sources driven organic Rankine cycle optimization. Appl Energy 2022;307:118277.
[49] Xu GQ, Fu J, Quan YK, Wen J, Dong BS. Experimental investigation on heat transfer characteristics of hexamethyldisiloxane (MM) at supercritical pressures for medium/high temperature ORC applications. Int J Heat Mass Tran 2020;156:119852.
[50] Weiß AP, Popp T, Zinn G, Preißinger M, Brüggemann D. A micro-turbine-generator-construction-kit (MTG-c-kit) for small-scale waste heat recovery ORC-Plants. Energy 2019;181:51–5.
[51] Xu L, Yuan JQ. Online application oriented calculation of the exhaust steam wetness fraction of the low pressure turbine in thermal power plant. Appl Therm Eng 2015;76:357–66.
[52] Cataldo F, Mastrullo R, Mauro AW, Vanoli GP. Fluid selection of organic Rankine cycle for low-temperature waste heat recovery based on thermal optimization. Energy 2014;72:159–67.
[53] Calise F, Capuozzo C, Carotenuto A, Vanoli L. Thermoeconomic analysis and off-design performance of an organic Rankine cycle powered by medium-temperature heat sources. Sol Energy 2014;103:595–609.
[54] HTRI Software. http://www.htri.net. [Accessed 19 January 2022].
[55] https://www.aspentech.com/en/products/engineering/aspen-plus. [Accessed 19 January 2022].
[56] EnergyPlus. Weather Data 2017. https://energyplus.net/weather/. [Accessed 19 January 2022].
[57] Chaibakhsh A, Ghaffari A. Steam turbine model. Simulat Model Pract Theor 2008;16:1145–62.
[58] Turboden. Turboden ORC Technol 2020. http://www.turboden.com/turboden-orc-technology/1065/innovation. [Accessed 19 May 2022].

Nomenclature

A: aperture area, m^2
a: Baumann factor/heat loss coefficient
C: cost, $
c: incidence angle coefficient
c_p: specific heat capacity, kJ/ (kg·K)
D: diameter, mm
E: elasticity modulus, MPa
F: factor
H: height, m
h: enthalpy, kJ/kg/edge height, mm
I: solar irradiance, W/m^2
K: incidence angle modifier factor
L: length, m
M: mass, tonne
$\dot{m}$: mass flow rate, kg/s
P: price, $\$/m^2$ / $/kg / $/kWh
p: pressure, MPa
q: heat loss coefficient, W/m
$\dot{q}$: absorbed heat, kW
R: equivalent outer radius of spherical shell, mm
S: heat exchanger area, m^2
T: temperature, °C
t: time, hour
V: volume, m^3
v: speed, m/s /specific volume, m^3/kg
W: annual power output, kWh
$\dot{w}$: work, kW
Y: yield, $
y: steam wetness, %
δ: thickness, mm
ε: device efficiency, %
η: efficiency, %
θ: incidence angle, °
φ: welding coefficient
ρ: density, kg/m^3
$[\sigma]^t$: permissible stress

Abbreviation

CEPCI: Chemical Engineering Plant Cost Index
CORC: cascade organic Rankine cycle
CSP: concentrated solar power
DSG: direct steam generation
DVG: direct vapor generation
EPP: equivalent payback period
HTA: high temperature accumulator
HX: heat exchanger
IAM: incidence angle modifier
LTA: low temperature accumulator
ORC: organic Rankine cycle pump
P: pump
PTC: parabolic trough collector
SAM: System Advisor Model
SORC: steam-organic Rankine cycle
SRC: steam Rankine cycle
TV: throttle valve
V: valve

Subscript

0 … 14: number
a: ambient
add: added
av: average
b: binary
BM: bare module
cr: critical
cy: cylinder
d: heat discharge
DN: direct normal
e: electricity
eq: equivalent
g: generator/static
i: inner
in: inlet
l: liquid
loss: heat loss
M: heat loss
max: maximum
min: minimum
o: outer
OT: ORC turbine
opt: optical
out: outlet
p: pressure/purchased
pinch: pinch point
s: isentropic/sunshine/saturation
ST: steam turbine
st: standard
sh: superheated
v: vapor
w: water/wind